DOES OXYGEN ISOTOPIC HETEROGENEITY IN REFRACTORY INCLUSIONS AND THEIR WARK-LOVERING RIMS RECORD NEBULAR REPROCESSING? J. I. Simon[1], J. E. P. Matzel[2], S. B. Simon[3], P. K. Weber[2], L. Grossman[3], D. K. Ross[1,4], and I. D. Hutcheon[2]. [1]Center for Isotope Cosmochemistry and Geochronology, KR NASA Johnson Space Center, Houston, TX 77058, USA (Justin.I.Simon@NASA.gov), [2]Lawrence Livermore National Laboratory, Livermore, CA 94551, USA, [3]The University of Chicago, Chicago, IL 60637, USA, [4]JE-23 Jacobs/ESCG, P.O. Box 58477, Houston, TX 77058.

Introduction: Large systematic variations in O-isotopic compositions found within individual mineral layers of rims surrounding Ca-, Al-rich inclusions (CAIs) and at the margins of some CAIs imply formation from distinct environments [e.g., 1-3]. The O-isotope compositions of many CAIs preserve a record of the Solar nebula gas believed to initially be ^{16}O-rich ($\Delta^{17}O \leq -25‰$) [4-5]. Data from a recent study of the compact Type A Allende CAI, A37, preserve a diffusion profile in the outermost ~70 μm of the inclusion and show >25‰ variations in $\Delta^{17}O$ within its ~100 μm-thick Wark-Lovering rim (WL-rim) [3]. This and comparable heterogeneity measured in several other CAIs have been explained by isotopic mixing between the ^{16}O-rich Solar reservoir and a second ^{16}O-poor reservoir (probably nebular gas) with a "planetary-like" isotopic composition, e.g., [1,2,3,6]. However, there is mineralogical and isotopic evidence from the interiors of CAIs, in particular those from Allende, for parent body alteration. At issue is how to distinguish the record of secondary reprocessing in the nebula from that which occurred on the parent body. We have undertaken the task to study a range of CAI types with varying mineralogies, in part, to address this problem.

Description of Studied CAIs: As part of a larger investigation to understand the fine scale O-isotopic records contained in CAIs and their surrounding rims, we report new profiles traversing the rims and margins of two Allende CAIs: Egg-6 (Type B1) and ALH3 (Type A), and compare them to the zoning profiles we have observed in Allende A37 (Type A) [3] & TS4 (Type B1) and the Efremovka CAI EF-1 (Type A) [7]. EF-1 contains almost no alteration products, typical of inclusions from the reduced subgroup of CV3 [8].

Egg-6 contains fassaite+anorthite+spinel+melilite in its core and has a well-developed melilite mantle [9]. The outer ~40 μm is made of a simple rim of Fe-rich spinel enclosing a semi-continuous chain of isolated perovskite crystals and a discontinuous layer of Al-rich pyroxene (Fig. 1). The Fe content of the spinel decreases inward towards the melilite mantle.

ALH3 contains melilite+anorthite+spinel in its interior [10]. Surrounding the CAI is a ~30 to 75 μm thick rim that exhibits: (1) secondary anorthite, (2) spinel, (3) Ti-pyx, (4) nepheline (discontinuous layer), (5) Al-diopside, and (6) Fe-rich olivine, ~Fa_{50}, which may be accreationary. ALH3 has a second "inner" rim sequence lining an extensive "pocket" (varying from ~50 to 100 μm thick) of: (1) secondary anorthite (discontinuous layer of varying thickness), (2) spinel (enclosing perovskite), (3) Ti-pyx, (4) Al-diopside, and (5) andradite. The primary difference between the sequences is the outermost layer phase (i.e., Fe-rich olivine versus andradite).

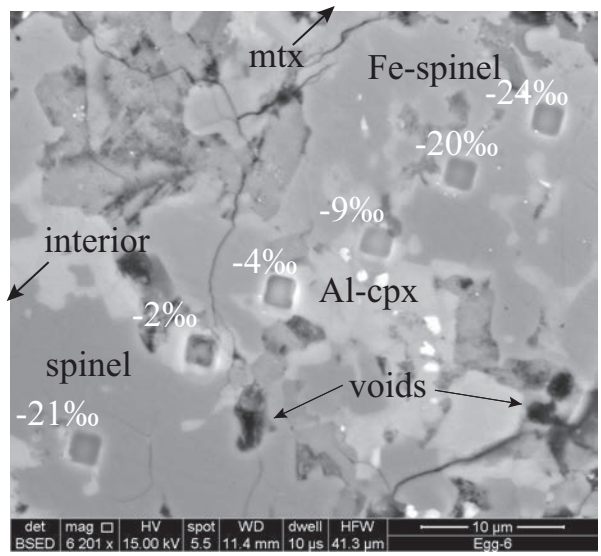

Figure 1. *Backscattered electron image of simple spinel-dominated rim surrounding Allende CAI Egg-6, obtained after NanoSIMS analysis. Chondrite matrix is located to upper right and melilite mantle and core of CAI to the lower left. $\Delta^{17}O$ shifts to less ^{16}O-rich values inward across the outer rim until the ^{16}O-rich inner spinel layer. Melilite interior is uniformly $\Delta^{17}O$ = -2 to -5‰.*

Methods: We used the LLNL NanoSIMS 50 to perform O-isotopic measurements following published methods [3]. O-isotope compositions are reported in terms of $\delta^{17}O$ and $\delta^{18}O$, reflecting the per mil difference from the standard mean ocean water (SMOW) such that $\delta^{i}O=10^{3}((^{i}O/^{16}O)/(^{i}O/^{16}O)_{SMOW}-1)$, where i is either 17 or 18. Based on terrestrial standard analyses, the external precision was <4.4‰ (2sd) for both ratios. $\Delta^{17}O$, defined as $\Delta^{17}O=\delta^{17}O-0.52x\delta^{18}O$, represents the departure from the terrestrial mass fractionation (TMF) line that defines the terrestrial oxygen reservoir. The difference in $\Delta^{17}O$ among the terrestrial minerals was

<0.5‰, much less than our typical uncertainty (~3.0‰). Mineral compositions, X-ray, and backscattered electron maps were used to guide NanoSIMS traverses and verify the mineralogy of analysis spots.

Results: Here we report O-isotope data for Egg-6 and ALH-3. These data come from ~2 µm spot analyses along traverses across their rims and into their interiors (Figs. 2, 3). All data reflect spots that come from a single mineral phase as evaluated by their $^{28}Si/^{16}O$ ion ratios and post-NanoSIMS SEM analyses, unless stated otherwise. Like previously studied CAIs, data from both Egg-6 and ALH-3 exhibit heterogeneous ^{16}O abundances (>20‰). Compared to A37, the interior melilites of both inclusions are uniformly ^{16}O-poor, $\Delta^{17}O$ = -2 to -5‰. Secondary anorthite at the margin of both CAIs has planetary-like, ^{16}O-poor compositions. Although some differences exist, the rims on Egg-6 and ALH-3 yield a similar isotopic stratigraphy to that found previously: spinel is ^{16}O-rich ($\Delta^{17}O \leq$-15‰); pyroxene often becomes relatively ^{16}O-poor towards the interior; and olivine varies in $\Delta^{17}O \geq$25‰. If present, voids and/or secondary mineralization tend to be located between mineral layers, e.g., spinel and pyx in rim of Egg-6 (Fig. 1). The traverse across the outer rim of ALH-3 was made where no secondary mineralization was observed.

Discussion: The new O-isotopic zoning profiles can be interpreted within the context of the zoning that we found previously but cannot be explained by O-isotope exchange controlled volume diffusion alone [i.e., 12]. The scale of variability is too great and the zoning is often reverse from that expected for exchange with an external ^{16}O-poor reservoir. The reverse zoning could be explained by fluid-mediated preferential transport of oxygen from elsewhere on the parent body to regions between preexisting mineral layers in the rim. Alternatively, the reverse zoning may reflect a record of oxygen isotope zoning of varying nebular gas. O-isotope exchange on parent bodies may account for some of the heterogeneity found within CAIs and their rims but has difficulty explaining: (1) the sense of reverse zoning found in pyroxene and spinel within WL rims (e.g., A37 and this study); (2) the lack of correlation between the inferred degree of exchange of the melilite interiors with degree of secondary mineralization (cf. those studied herein as compared to alteration free, but completely exchanged EF-1 [7]); (3) the reverse zoning of the melilite interior found in EF-1 and possibly ALH-3 (Fig. 3); and (4) the T (>1100 K) and time (>5 Ma) conditions required to explain the O-isotope zoning in A37 by volume diffusion [3]. More work is required to identify patterns in isotopic variation, to verify the existence of nebular reprocessing events, and to determine how and where they may have occurred within the protoplanetary disk.

References: [1] Itoh S. and H. Yurimoto (2003) *Nature*, 423, 728-731. [2] Aleon, J. et al. (2007) *EPSL,* 263, 114-127. [3] Simon, J.I. et al. (2011) *Science*, 331, 1175-1178. [4] Aléon, J. et al. (2002) *MPS*, 37, 1729-1755. [5] McKeegan, K.D. et al. (2011), *Science* 332, 1528-1532. [6] Clayton, R.N. et al. (1977) *EPSL* 34, 209-224. [7] Simon, J. I. et al. (2012) *LPS XLIII* Abs #1340. [8] Simon, S. et al. 1999 *GCA* 63, 1233-1248. [9] Meeker, G. P. et al. (1983) *GCA,* 47, 707-721. [10] Simon, S. et al., (2001) *MAPS* 36, 331-350. [11] Matzel et al., (2011) *LPI Cont.* #1639. [12] Ryerson, F.J. and K.D. McKeegan (1994) *GCA* 58, 3713-3734.

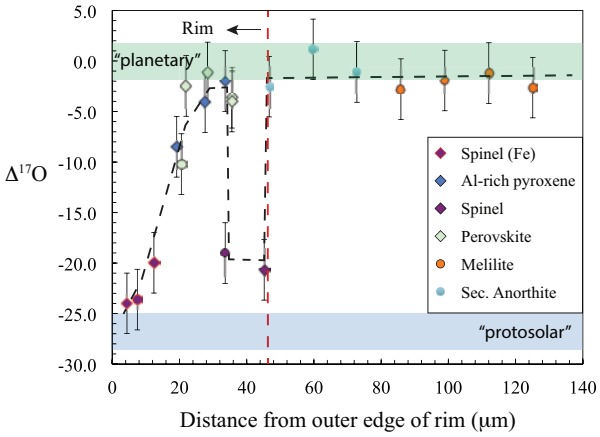

Figure 2. *O-isotope zoning profile across rim of Allende CAI Egg-6. No olivine in rim, similar to that observed for EF-1. Rim exhibits reverse zoning assuming exchange with a ^{16}O-poor ('planetary') reservoir. Secondary anorthite shares the uniform composition of the melilite (a trend that extends inward for across Egg-6 for >500 µm, see [11]).*

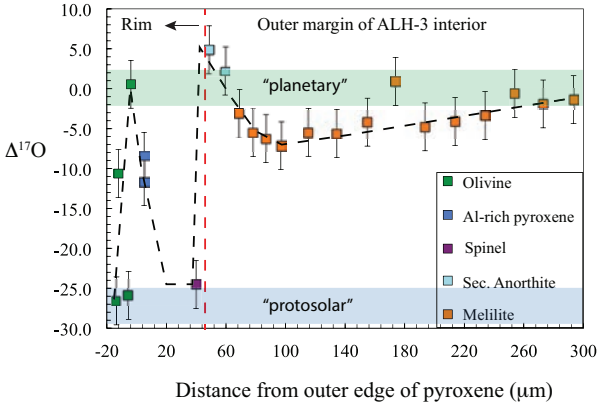

Figure 3. *O-isotope zoning profile across WL-rim and margin of Allende CAI ALH-3. Melilite is similar to Egg-6 [11] and EF-1 [7]; WL-rim is similar to A37 [3] and TS4 [7].*